Exploration for the Self-ordering of Porous Alumina Fabricated via Anodizing in Etidronic Acid

Akimasa Takenaga, Tatsuya Kikuchi*,[1], Shungo Natsui, and Ryosuke O. Suzuki
Faculty of Engineering, Hokkaido University
N13-W8, Kita-ku, Sapporo, Hokkaido, 060-8628, Japan

*Corresponding author: Tatsuya Kikuchi
TEL: +81-11-706-6340
FAX: +81-11-706-6342
E-mail: kiku@eng.hokudai.ac.jp

[1] ISE active member

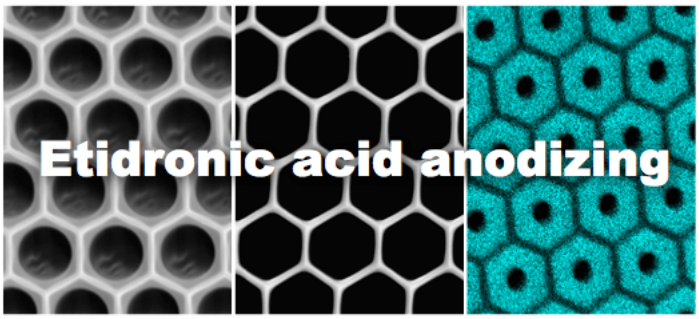

Graphical abstract

Highlights

Etidronic acid anodizing caused self-ordering behaviors between 165 and 270 V.

Large-scale pore arrays measuring 470 nm in diameter could be fabricated.

Hexagonal phosphorus-free distribution was measured in the porous alumina.

A truly honeycomb alumina structure consisting of hexagonal pores was formed.

Abstract

Ordered porous alumina (OPA) with large-scale circular and hexagonal pores was fabricated via etidronic acid anodizing. High-purity aluminum plates were anodized in 0.2-4.2 M etidronic acid solution at 145-310 V and 288-323 K. Self-ordering of porous alumina was observed at 165 V and 313 K in 4.2 M, at 205 V and 303 K in 1.0 M, and at 260 V and 298 K in 0.2 M, and the cell diameter was measured to be 400-640 nm. The ordering potential difference decreased with the electrolyte concentration increasing. OPA without an intercrossing nanostructure could be fabricated on a nanostructured aluminum surface via two-step anodizing. Subsequent pore-widening in etidronic acid solution caused the circular dissolution of anodic oxide and the expansion of pore diameters to 470 nm. The shape of the pores was subsequently changed to a hexagon from a circle via long-term pore-widening, and a honeycomb structure with narrow alumina walls and hexagonal pores measuring 590 nm in its long-axis was formed in the porous alumina. Transition of the nanostructure configuration during pore-widening corresponded to differences in the incorporated phosphorus distribution originating from the etidronic acid anions.

Keywords: Aluminum; Anodizing; Etidronic Acid; Porous Alumina; Self-Ordering

1. Introduction

Anodizing of aluminum and its alloys under appropriate electrochemical conditions allows the formation of ordered porous alumina (OPA) with nanoscale honeycomb structures on aluminum substrates [1-6]. OPA has many nanoscale pores with a high regularity, and can be easily fabricated via a simple anodizing technique without any special equipment or technique such as photolithography, electron-beam lithography, and nanoimprinting (self-ordering). Therefore, it is widely used by many researchers as a template for novel and challenging nanodevices in the fields of electronic and optical applications [7-14]. It is a well-known experimental fact that the periodic size of the OPA, which is called the "cell size" or "interpore distance", strongly depends on the applied potential difference (voltage) and electrolyte species used for anodizing in the aqueous solutions [2,5,15,16]. Sulfuric acid at an ordering potential difference of 19 V (corresponding cell size: 50 nm) - 25 V (60 nm) [4,5,17-19], oxalic acid at 40 V (100 nm) [4,5,20], selenic acid at 42 V (95 nm) - 48 V (112 nm) [21-23], malonic acid at 120 V (300 nm) [24], phosphonic acid at 150 V (370 nm) - 180 V (440 nm) [25], phosphoric acid at 160 V (405 nm) - 195 V (500 nm) [26,27], and tartaric acid at 195 V (500 nm) [24] have been reported as anodizing electrolytes to date. The bottom shape of the porous alumina exhibits a self-ordered cell structure as a result of rearrangement of the initially disordered cells under the potential difference applied [2].

OPA with large-scale cell sizes and pores is required for expanding the application field in nano- and micro-structure fabrication [28,29]. Recently, we reported an OPA formed via anodizing in the novel electrolyte etidronic acid (1-hydroxyethane-1,1-diphosphonic acid, $CH_3C(OH)[PO(OH)_2]_2$) [30]. Etidronic acid anodizing at 210-270 V at appropriate temperatures caused the self-ordering behavior of porous alumina, and OPA with large-scale cell diameters of 530-670 nm could be successfully fabricated on aluminum substrates. An ordered aluminum dimple array created from etidronic acid anodizing and subsequent selective oxide dissolution led to a bright structural coloration with a rainbow spectrum due to submicrometer-scale periodic structures. We demonstrated the transfer of the ordered nanostructures to polydimethylsiloxane (PDMS) and ultraviolet (UV) curable polymers via nanoimprinting [31]. In these previous investigations, whole anodizing investigations were carried out in a 0.3 M etidronic acid solution, which is a frequently used electrolyte concentration for anodizing including other electrolyte solutions such as sulfuric, oxalic, and phosphoric acid [17,20,26]. In contrast, we found that anodizing at

different electrolyte concentrations expanded the ordering potential difference and corresponding cell size ranges [22,25]. Therefore, etidronic acid anodizing in various electrolyte concentrations may exhibit undiscovered self-ordering at potential differences over 210-270 V.

In the present investigation, we demonstrated etidronic acid anodizing at various electrolyte concentrations and electrochemical operating conditions. OPA with large-scale cell sizes and pore diameters was successfully fabricated via two-step etidronic acid anodizing and subsequent pore-widening. Evaluation and characterization of the OPA, including its nanostructures and elemental distributions, were investigated via high-resolution electron microscopy. A unique honeycomb nanostructure with narrow alumina walls could be fabricated via long-term slow pore-widening and based on the hexagonal distribution of the phosphorus originating from the electrolyte.

2. Experimental

High-purity aluminum plates (99.999 wt%, 0.25-1.0 mm thick, GoodFellow, UK) were cut into 10 mm × 20 mm pieces with a handle. The aluminum pieces were ultrasonically degreased in ethanol for 10 min at room temperature. The lower half of the handle of the aluminum specimen was coated with a silicone resin (KE45W, Shin-Etsu, Japan) to avoid the electrochemical reaction on the handle. Prior to silicone resin coating, the aluminum surface on the coated region was mechanically polished with a SiC paper for adhesion improving. After resin coating, the specimens were immersed in a 13.6 M CH_3COOH/2.56 M $HClO_4$ (78 vol% CH_3COOH/22 vol% 70% $HClO_4$) solution at 280 K and were electropolished at 28 V for 1-10 min. A large aluminum plate (99.99 wt%, Nippon Light Metal, Japan) was used as the cathode, and the solution was slowly stirred with a magnetic stirrer during electropolishing. After electropolishing, the specimens were washed with distilled water and then stored in a drying container.

The electropolished specimens were immersed in 0.2-4.2 M etidronic acid solution (150 mL, Tokyo Chemical Industry, Japan) at 288-323 K and then anodized at 145-310 V for up to 24 h using a direct power supply (PWR400H, Kikusui Electronics, Japan) connected to a PC. In the initial stage of anodizing, the potential difference was linearly increased for the first 2.5 min to avoid oxide burning phenomenon as much as possible, and then held at each target potential difference. The inner diameter of the electrochemical cell used for anodizing was 55 mm. A platinum plate (26 mm × 15 mm,

99.95 wt%, Nilaco, Japan) was used as the cathode and was set 15 mm apart from and parallel to the aluminum specimen. The solution was vigorously stirred with a cross-head stir bar. The current density was measured by a digital multimeter (DMM4040, Tektronix, USA) during the anodizing. Details of the anodizing setup have been shown elsewhere [16]

After anodizing, the anodic oxide formed on the aluminum specimens was selectively dissolved in a 0.2 M CrO_3/0.51 M H_3PO_4 solution at 353 K to expose the aluminum substrate. The nanoscale aluminum dimple array corresponding to the negative shape of the bottom of the porous alumina was formed on the aluminum substrate. The extent of the self-ordering behavior was evaluated by fast Fourier transform (FFT). The nanostructured aluminum specimens were anodized again in etidronic acid solution under the same anodizing conditions to fabricate the OPA (two-step anodizing). This process was carried out for the formation of OPA with whole vertical regions. After the two-step anodizing, the specimens were immersed in a 1.0 M etidronic acid solution at 298 K for up to 72 h to expand the diameter of the pores in the OPA (pore-widening).

The aluminum specimens in each step were examined by field emission scanning electron microscopy (FE-SEM, JSM-6500F and JIB-4600F/HKD, JEOL, Japan). For the observation of anodic oxide, a thin platinum electroconductive layer was coated onto the anodic oxide with a platinum sputter coater (MSP-1S, Vacuum Device, Japan). OPA fabricated via two-step anodizing was also examined by image-aberration-corrected scanning transmission electron microscopy (STEM, Titan G2 60-300, 300 kV, FEI). For the STEM observation, specimen preparation was carried out with the following four steps: 1) porous alumina on one side of the specimen was completely dissolved in a 2.5 M NaOH solution at room temperature to expose the aluminum substrate; 2) the specimens were immersed in a 0.5 M $SnCl_4$ solution at room temperature to completely dissolve the aluminum substrate and a free-standing porous alumina film without the aluminum substrate was obtained via the chemical dissolution processes; 3) the oxide film was pasted on a molybdenum single-hole grid (Nisshin EM, Japan) with an epoxy resin, and 4) the oxide layer was thinned by an argon ion beam using a precision ion polishing system (PIPS, Gatan). The distribution of aluminum, oxygen, phosphorus, and carbon in the porous alumina was examined by STEM-energy dispersive X-ray spectrometry (EDS).

3. Results and Discussion

3.1 Anodizing in a low concentration etidronic acid solution

The current-time curves during anodizing of aluminum in etidronic acid were investigated to fabricate OPA. Figure 1 shows changes in the current density, j, with the anodizing time, t, at potential differences of U = 255-265 V in a 0.2 M etidronic acid solution at 298 K. Because the potential difference increased linearly for the first 2.5 min to avoid sudden oxide burning, steady current densities measuring approximately 50 Am^{-2} were measured during the initial stage of anodizing. At this stage, barrier anodic oxide with the initial nanopores was formed [2]. As the potential differences reached each constant value after 2.5 min, the current densities rapidly dropped to approximately 10 Am^{-2}. After dropping, the current densities gradually increased due to the initial formation of nanopores in the anodic oxide film. While anodizing at 255 V and 260 V, the current densities reached steady values for the steady growth of porous alumina. The steady current density increased with the applied potential differences due to the rapid growth of the porous alumina which was approximately 100 Am^{-2} at 255 V to 130 Am^{-2} at 260 V. As the applied potential difference increased to 265 V, the current density increased more rapidly to above 200 Am^{-2} during the first 15 min and gas was vigorously generated from the surface of the aluminum specimen. Non-uniform oxide spots with a dark brown hue were partially observed on the specimen anodized under the high potential difference. This non-uniform oxide formation with many cracks is known as the oxide burning phenomenon [32-35], and uniform porous alumina could not be obtained on the aluminum surface under the oxide burning condition. Therefore, the maximum potential difference without oxide burning in 0.2 M etidronic acid solution at 298 K was determined to be 260 V from the electrochemical measurements (Fig. 1).

Previous investigations have shown that OPA can be typically fabricated via anodizing at maximum potential difference without oxide burning [24, 25]. Thus, the maximum potential differences for a 0.2 M etidronic acid solution at 288-323 K were investigated via the same anodizing method. The current densities under anodizing at maximum potential difference are summarized in Figure 2. The maximum potential difference without oxide burning at 288 K was determined to be a relatively high potential difference of 310 V. This decreased gradually with increasing solution temperatures and was determined to be 205 V at 323 K. This is due to the thinning of the barrier layer at the bottom of the porous alumina in the high temperature acidic

environments. The current density increased with the solution temperature. Although a relatively high current density of approximately 470 Am^{-2} was measured in the initial stage of anodizing at 205 V and 323 K, no oxide burning was observed on the specimen surface because of the immediate decrease in current density after the initial stage. The self-ordering behavior in these maximum potential differences was investigated by SEM observations.

Figure 3a shows an SEM image of the surface of the specimen anodized in a 0.2 M etidronic acid solution at 303 K and 240 V for 120 min, which is described in Fig. 2. Numerous nanopores measuring several tens of nanometers in diameter were disorderly formed on the surface of the anodic oxide. Because the nanopores are formed in a disorderly fashion during the initial stage of anodizing, irregularly arranged nanopores are observed [16]. To observe the growth plane of the porous alumina, i.e., the interface between the porous alumina and the aluminum substrate, anodic oxide was selectively dissolved in a CrO_3/H_3PO_3 mixture solution at 353 K. The exposed aluminum surface is shown in Fig. 3b. A submicrometer-scale aluminum dimple array corresponding to the bottom shape of the porous alumina can be observed on the surface, and each dimple, which measured approximately 590 nm in diameter, was regularly arranged. Therefore, the porous alumina was ordered during anodizing under this anodizing condition. In our investigation, self-ordering of the porous alumina was defined by the formation of an ideal cell arrangement containing more than 50 hexagonal cells.

Figure 4 shows SEM images of the typical aluminum surface obtained by anodizing in 0.2 M etidronic acid solution at 205-310 V (Fig. 2). An ideal dimple arrangement measuring 640 nm in dimple diameter was successfully obtained via anodizing at 260 V (Fig. 4b). Conversely, a disordered dimple array with many different cell diameters was formed at higher potential differences of 300 V (Fig. 4c) and 310 V (Fig. 4d), though large-scale cell diameters above 500 nm were also measured under these high potential differences. Thus, no ordering of the porous alumina can be confirmed via etidronic acid anodizing under these conditions. It was previously reported that long-term anodizing under ordering conditions improved the regularity of porous alumina due to the rearrangement of the porous alumina [1]. Therefore, 24-hour anodizing at the same potential differences of 300 V and 310 V was also conducted to improve its regularity. However, similarly disordered dimple arrays were observed on the aluminum surface after long-term anodizing (Figs. 4c and 4d, right figures). By anodizing at 300 V and 310 V, the current densities during steady-state growth are

smaller than that at 240 V and 260 V, being below 100 Am^{-2} (Fig. 2). In such low current density conditions, ordering may not be achieved due to low viscous flow of the anodic oxide during anodizing [24,36-38]. An SEM image of an aluminum dimple array fabricated via anodizing in 0.2 M etidronic acid solution at 205 V and 323 K is shown in Fig. 4a. Although a high current density (150-470 Am^{-2}) was measured during anodizing at 205 V (Fig. 2), disordered dimple arrays were also observed on the aluminum substrate. The porous alumina has a branching colonial structure due to the active chemical dissolution of anodic oxide in etidronic acid solution at such high temperatures. Therefore, it may be difficult to obtain the OPA under high temperature etidronic acid anodizing such as 323 K. In summary, the ordering region could be determined to be 240-260 V for 590-640 nm cell sizes when anodizing in 0.2 M etidronic acid at 298-303 K.

3.2 Anodizing in a high concentration etidronic acid solution

To expand the ordering region of etidronic acid anodizing, electrochemical behavior was also investigated via anodizing in 1.0-4.2 M etidronic acid solutions. It was expected that the decrease in the ordering potential difference region would occur by etidronic acid anodizing. As a result, the appropriate anodizing conditions such as temperature were significantly changed. Therefore, the maximum potential difference anodizing under various different conditions were investigated to fabricate OPA. Figure 5 shows the current-time curves at 145-245 V and 293-323 K in 1.0 M and 4.2 M etidronic acid solutions under the maximum potential differences. The following similar electrochemical behaviors were measured during etidronic acid anodizing at these high concentrations: 1) the maximum potential differences without oxide burning decreased with solution temperature and 2) the current density increased with solution temperature. In contrast, although the concentration of the solution is high, the current densities measured in 4.2 M etidronic acid solution were considerably lower than those in 0.2 M and 1.0 M solutions. This decrease may be due to the conductivity of the electrolyte solutions; 8.48 Sm^{-1} in 4.2 M etidronic acid solution at 298 K and 9.95 Sm^{-1} in 1.0 M at 298 K. The regularity of the aluminum dimple array under these anodizing conditions was also investigated by SEM observations.

Figure 6 shows SEM images of the aluminum dimple array fabricated with 1.0 M etidronic acid anodizing at 170-245 V and 293-323 K (the current-time curves were shown in Fig. 5a). Ideal dimple arrangements with more than 50 dimples and the

following anodizing conditions were observed on the aluminum surface via these operating conditions: 1) 520 nm at 215 V, 2) 520 nm at 205 V, and 3) 500 nm at 200 V. In contrast, ordered and disordered structures were mixed on the aluminum specimens anodized at 185 V and 313 K. The dimple array was also clearly disordered over the aluminum surface under the following anodizing conditions: 1) 245 V and 293 K and 2) 170 V and 323 K. It is difficult to fabricate OPA at these low and high temperatures, which is similar to 0.2 M etidronic acid solution. The ordering region was determined to be 200-215 V for 500-530 nm diameters in the 1.0 M etidronic acid solution, and it expanded with lower potential differences using a high concentration solution.

As the concentration increased to 4.2 M, which is a commercially available high concentration etidronic acid, it is possible to further expand the ordering region. Figure 7a shows an SEM image of an aluminum surface after 4.2 M etidronic acid anodizing at 165 V and 313 K for 24 h. An aluminum dimple measuring 400 nm in diameter was ideally arranged on the surface. However, an irregular dimple array was observed in 4.2 M etidronic acid anodizing under other operating conditions (Fig. 7b). Figure 8 shows SEM images of ordered dimple arrays on wider view fields. The resulting FFT image of each specimen exhibited a spot pattern based on the ordered nanostructure. However, several disordered pores were also observed on the wider field. For the formation of OPA with higher regularity, it may be useful to combine nanoimprinting techniques with anodizing. The experimental results show that anodizing at 165-260 V in 0.2-4.2 M etidronic acid solutions causes the ordering behavior of porous alumina with large-scale cell sizes measuring 400-640 nm in diameter. Considering our previous investigations in a 0.3 M etidronic acid solution, the ordering potential differences was determined to be 165-270 V for 400-670 nm. Therefore, the ordering of the porous alumina at a wide range of potential differences and corresponding cell sizes can be achieved through etidronic acid anodizing. Ordering behaviors at 165-270 V may be achieved by fine adjusting of the concentration and temperature.

3.3 Nanostructural engineering of self-ordered porous alumina

For various nanoapplications such as nanotemplates and nanofilters, two-step etidronic acid anodizing and subsequent pore-widening were carried out. Figure 9a shows an ordered dimple array fabricated via anodizing in a 0.2 M etidronic acid solution at 298 K and 260 V for 24 h, considering the experimental results described above. An ordered dimple array consisting of several hundred dimples measuring 640

nm in diameter was successfully fabricated via etidronic acid anodizing. For the fabrication of OPA through the vertical cross-section, the nanostructured aluminum specimen was anodized again in etidronic acid solution under the same conditions for 120 min (two-step anodizing). A high magnification SEM image of the OPA fabricated via two-step anodizing is shown in Fig. 9b. A hexagonal unit cell with a pore measuring 330 nm in diameter at its center was ideally distributed on the surface. A slight ledge at the lower right of each pore (yellow arrow shown in Fig. 9b) was formed in the initial stage of etidronic acid anodizing because the applied potential difference increased linearly during the first 2.5 min to avoid the oxide burning phenomenon due to the anodizing at high potential differences.

The OPA was immersed in an etidronic acid solution to expand the pore diameter (pore-widening). Phosphoric acid was generally used as the pore-widening solution in previous investigations [41-43]. However, a 1.0 M etidronic acid (pH = 0.79 at 298 K) was used as the etching solution to slowly dissolve the anodic oxide in our investigation. Figure 9c shows an SEM image of the surface of the porous alumina after the pore-widening process for 48 h. The shape of the pores in each unit cell expanded circularly via 48-h-pore-widening, and large-scale circular pores measuring 470 nm in diameter were fabricated in the porous alumina. Such large pores cannot be fabricated via phosphoric acid anodizing because the maximum hexagonal cell size is 500 nm [2]. Accordingly, OPA with large-scale pore diameters measuring 330-470 nm can be fabricated via pore-widening in etidronic acid solution for appropriate amounts of time and at specific solution temperatures. Interestingly, white honeycomb walls measuring 50-60 nm in width were clearly observed at the cell boundaries (Fig. 9c). Additionally, a narrow gray oxide with inner circular and outer hexagonal features was also located on the inside of the honeycomb walls. The details of these unique nanostructures will be discussed later. As the pore-widening time increased to 72 h (Fig. 9d), the gray oxide was completely dissolved into the etidronic acid solution, and an ideal honeycomb nanostructure with narrow alumina walls was fabricated. The lengths of both the long- and short-axis directions of the hexagonal pore were measured to be 590 nm and 540 nm, respectively, and large-scale pores above 500 nm in diameter could be formed. Notably, it is difficult to fabricate these unique hexagonal nanostructures via the high-speed chemical etching of anodic alumina because aluminum oxide was rapidly dissolved into the solution. Figures 9e-9g show the fracture cross-sections of the OPA. High aspect-ratio OPA without an intercrossing structure were successfully obtained.

The inner oxide in the porous layer was also dissolved into the solution by the pore-widening process, and a thinned barrier layer measuring 65 nm in thickness was also observed at the bottom of pores. Such a hexagonal pore array may be useful as a nanotemplate for the fabrication of hexagonal nanostructures [44].

For nanocharacterization of OPA fabricated via etidronic acid anodizing, the OPA was physically thinned via an argon ion beam. Figure 10 shows a SEM image, a TEM diffraction pattern, and STEM-EDS mapping images of the aluminum, oxygen, phosphorous, and carbon element distributions of the OPA. This OPA was fabricated via two-step etidronic acid anodizing at 298 K and 215 V, and the average diameter of the pores was measured to be approximately 160 nm in a SEM image. The TEM diffraction pattern showed that the porous alumina was amorphous, which is similar to typical porous alumina.

Although aluminum, oxygen, and carbon were distributed over the entire anodic oxide region, practically phosphorus-free cell boundaries with a honeycomb configuration were measured by STEM-EDS. Whereas the outer alumina around the pores contained approximately 3.5% phosphorus, the inner alumina with a hexagonal distribution contained 0.07% phosphorus. The shapes of the hexagonal alumina nanostructures shown in Figs. 9c and 9d may correspond to this phosphorus distribution. Generally, the chemical dissolution rate of anodic alumina increases with the amounts of incorporated anions originating from the electrolyte during anodizing. In fact, the successive fabrication of ordered through-hole porous alumina membranes due to differences in the dissolution rate has been reported by Yanagishita et al. [45] In our investigation, the following dissolution behavior can be considered during pore-widening: 1) the anodic oxide with incorporated phosphorus around the pores dissolves isotropically into etidronic acid solution, and large circular pores were formed in the porous alumina and 2) subsequent pore-widening causes the complete dissolution of the phosphorus containing anodic oxide, but phosphorus-free hexagonal alumina walls remains due to the slow dissolution rate.

Etidronic acid used as an anodizing electrolyte has two phosphorus atoms and two carbon atoms in the molecular structure. Etidronic acid is a tetra acid with the following acid dissociation constants (pKa) [46-47]:

$$C_2H_8O_7P_2 \rightleftarrows 4H^+ + C_2H_4O_7P_2^{4-}$$

($pKa_1 = 1.43$, $pKa_2 = 2.70$, $pKa_3 = 7.02$, $pKa_4 = 11.20$)

The anions that dissociate in the aqueous solution were incorporated into the anodic

oxide by a high electric field during anodizing [48-50]. Interestingly, the distribution of phosphorus and carbon elements originating from the anions is clearly different in the porous alumina from the STEM-EDS measurements; phosphorus was distributed in the honeycomb, while carbon was distributed uniformly in the oxide. The right of Fig. 10 shows an EDS spectrum measured for the OPA formed via anodizing in etidronic acid and sulphate (SO_4^{2-}) solutions. Here, these specimen preparations were carried out with the same procedure at the same time for the STEM observations. There is a clear peak for carbon only in the porous alumina formed via etidronic acid anodizing. Therefore, it is difficult to explain the reason of the uniform carbon distribution with hydrocarbon contaminants, and the distribution may show the carbon elements incorporated in the porous alumina. These different distributions of carbon and phosphorus may suggest that the chemical bonds of incorporated anions with a large molecular structure are cleaved in the anodic oxide during incorporation. Whether anions decompose or not depend on the electrolyte spices used. However, there is no direct evidence supporting the molecular structure of etidronic acid in the porous alumina, and the chemical-bonding state of the molecules should be further investigated to better understand anion incorporation during anodizing in etidronic acid.

4. Conclusions

We demonstrated the self-ordering behavior of porous alumina fabricated via etidronic acid solution, and the resulting nanostructures were investigated in details. Self-ordering of porous alumina is observed over a wide range of potential differences (at 165 V and 313 K in 4.2 M, at 205 V and 303 K in 1.0 M, and at 260 V and 298 K in 0.2 M), and the formation of OPA measuring 400-640 nm in cell diameter can be achieved. A hexagonal phosphorus-free distribution was formed in the OPA fabricated via two-step 1.0 M etidronic acid anodizing at 215 V and 298 K for 24 h and 120 min. A honeycomb nanostructure with hexagonal pores can be fabricated via long-term pore-widening, and the lengths of both the long- and short-axis directions of the hexagonal pore were measured to be 590 nm and 540 nm, respectively. The shape of this honeycomb nanostructure corresponds to the phosphorus distribution in the porous alumina.

Acknowledgments

This study was conducted at Hokkaido University and was supported by the

“Nanotechnology Platform” Program of the Ministry of Education, Culture, Sports, Science, and Technology (MEXT), Japan. The authors would like to thank Mr. Nobuyuki Miyazaki, Mr. Takashi Endo, and Mr. Ryo Oota for their assistance in the SEM and STEM observations. This study was financially supported by the Light Metal Educational Foundation and the Sumitomo Foundation (No. 151181), Japan.

References

1) H. Masuda, K. Fukuda, Ordered metal nanohole arrays made by a two-step replication of honeycomb structures of anodic alumina, Science 268 (1995) 1466.
2) W. Lee, S.-J. Park, Porous anodic aluminum oxide: anodization and templated synthesis of functional nanostructures, Chemical Reviews 114 (2014) 7487.
3) G.D. Sulka, Highly ordered anodic porous alumina formation by self-organized anodizing, in: A. Eftekhari (Ed.), Nanostructured Materials in Electrochemistry, Wiley-VCH, 2008, p. 1.
4) A.P. Li, F. Müller, A. Birner, K. Nielsch, U. Gösele, Hexagonal pore arrays with a 50–420 nm interpore distance formed by self-organization in anodic alumina, Journal of Applied Physics 84 (1998) 6023.
5) W. Lee, R. Ji, U. Gösele, K. Nielsch, Fast fabrication of long-range ordered porous alumina membranes by hard anodization, Nature Materials 5 (2006) 741.
6) M. Michalska-Domańska, M. Norek, W.J. Stępniowski, B. Budner, Fabrication of high quality anodic aluminum oxide (AAO) on low purity aluminum—A comparative study with the AAO produced on high purity aluminum, Electrochimica Acta 105 (2013) 424.
7) T. Ozel, G.R. Bourret, C.A. Mirkin, Coaxial lithography, Nature Nanotechnology 10 (2015) 319.
8) A. Mozalev, M. Bendova, R.M. Vazquez, Z. Pytlicek, E. Llobet, J. Hubalek, Formation and gas-sensing properties of a porous-alumina-assisted 3-D niobium-oxide nanofilm, Sensors and Actuators B: Chemical 229 (2016) 587.
9) M. Ahmadzadeh, M. Almasi-Kashi, A. Ramazani, A.H. Montazer, Electrodeposition efficiency of Ni in the fabrication of highly ordered nanowire arrays: The roles of Cu pre-plating and barrier layer temperature, Applied Surface Science 356 (2015) 687.
10) A. Mozalev, R.M. Vázquez, C. Bittencourt, D. Cossement, F. Gispert-Guirado, E. Llobet, H. Habazaki, Formation–structure–properties of niobium-oxide nanocolumn arrays via self-organized anodization of sputter-deposited aluminum-on-niobium

layers, Journal of Materials Chemistry C 2 (2014) 4847.
11) W.J. Stępniowski, M. Norek, M. Michalska-Domańska, Z. Bojar, Ultra-small nanopores obtained by self-organized anodization of aluminum in oxalic acid at low voltages, Materials Letters 111 (2013) 20.
12) M.A. Kashi, A. Ramazani, H. Abbasian, A. Khayyatian, Capacitive humidity sensors based on large diameter porous alumina prepared by high current anodization, Sensors and Actuators A: Physical 174 (2012) 69.
13) G.D. Sulka, K. Hnida, Distributed Bragg reflector based on porous anodic alumina fabricated by pulse anodization, Nanotechnology 23 (2012) 075303.
14) H. Masuda, M. Yamada, F. Matsumoto, S. Yokoyama, S. Mashiko, M. Nakao, K. Nishio, Lasing from Two-Dimensional Photonic Crystals Using Anodic Porous Alumina, Advanced Materials 18 (2006) 213.
15) S.Z. Chu, K. Wada, S. Inoue, M. Isogai, Y. Katsuta, A. Yasumori, Large-scale fabrication of ordered nanoporous alumina films with arbitrary pore intervals by critical-potential anodization, Journal of the Electrochemical Society 153 (2006) B384.
16) T. Kikuchi, D. Nakajima, O. Nishinaga, S. Natsui, R.O. Suzuki, Porous aluminum oxide formed by anodizing in various electrolyte species, Current Nanoscience 11 (2015) 560.
17) H. Masuda, F. Hasegwa, S. Ono, Self-ordering of cell arrangement of anodic porous alumina formed in sulfuric acid anodizing, Journal of The Electrochemical Society 144 (1997) L127.
18) G.D. Sulka, K.G. Parkoła, Temperature influence on well-ordered nanopore structures grown by anodization of aluminium in sulphuric acid, Electrochimica Acta 52 (2007) 1880.
19) G.D. Sulka, S. Stroobants, V. Moshchalkov, G. Borghs, J.P. Celis, Synthesis of well-ordered nanopores by anodizing aluminum foils in sulfuric acid, Journal of the Electrochemical Society 149 (2002) D97.
20) O. Jessensky, F. Müller, U. Gösele, Self-organized formation of hexagonal pore arrays in anodic alumina, Applied Physics Letters 72 (1998) 1173.
21) O. Nishinaga, T. Kikuchi, S. Natsui, R.O. Suzuki, Rapid fabrication of self-ordered porous alumina with 10-/sub-10-nm-scale nanostructures by selenic acid anodizing, Scientific reports 3 (2013) 2748.
22) T. Kikuchi, O. Nishinaga, S. Natsui, R.O. Suzuki, Self-ordering behavior of anodic

porous alumina via selenic acid anodizing, Electrochimica Acta 137 (2014) 728.
23) S. Akiya, T. Kikuchi, S. Natsui, R.O. Suzuki, Optimum exploration for the self-ordering of anodic porous alumina formed via selenic acid anodizing, Journal of The Electrochemical Society 162 (2015) E244.
24) S. Ono, M. Saito, H. Asoh, Self-ordering of anodic porous alumina formed in organic acid electrolytes, Electrochimica Acta 51 (2005) 827.
25) S. Akiya, T. Kikuchi, S. Natsui, N. Sakaguchi, R.O. Suzuki, Self-ordered porous alumina fabricated via phosphonic acid anodizing, Electrochimica Acta 190 (2016) 471.
26) H. Masuda, K. Yada, A. Osaka, Self-ordering of cell configuration of anodic porous alumina with large-size pores in phosphoric acid solution, Japanese Journal of Applied Physics 37 (1998) L1340.
27) K. Nielsch, J. Choi, K. Schwirn, R.B. Wehrspohn, U. Gösele, Self-ordering regimes of porous alumina: The 10% porosity rule, Nano Letters 2 (2002) 677.
28) X. Chen, D. Yu, L. Gao, X. Zhu, Y. Song, H. Huang, L. Lu, X. Chen, Fabrication of ordered porous anodic alumina with ultra-large interpore distance using ultrahigh voltages, Materials Research Bulletin 57 (2014) 116.
29) Q. Lin, B. Hua, S.F. Leung, X. Duan, Z. Fan, Efficient light absorption with integrated nanopillar/nanowell arrays for three-dimensional thin-film photovoltaic applications, ACS Nano 7 (2013) 2725.
30) T. Kikuchi, O. Nishinaga, S. Natsui, R.O. Suzuki, Fabrication of self-ordered porous alumina via etidronic acid anodizing and structural color generation from submicrometer-scale dimple array, Electrochimica Acta 156 (2015) 235.
31) T. Kikuchi, O. Nishinaga, S. Natsui, R.O. Suzuki, Polymer nanoimprinting using an anodized aluminum mold for structural coloration, Applied Surface Science 341 (2015) 19.
32) K. Schwirn, W. Lee, R. Hillebrand, M. Steinhart, K. Nielsch, U. Gösele, Self-ordered anodic aluminum oxide formed by H_2SO_4 hard anodization, ACS Nano 2 (2008) 302.
33) T. Aerts, I. De Graeve, H. Terryn, Study of initiation and development of local burning phenomena during anodizing of aluminium under controlled convection, Electrochimica Acta 54 (2008) 270.
34) T. Aerts, I. De Graeve, H. Terryn, Anodizing of aluminium under applied electrode temperature: Process evaluation and elimination of burning at high current densities,

Surface and Coatings Technology 204 (2010) 2754.
35) S. Ono, M. Saito, H. Asoh, Self-ordering of anodic porous alumina induced by local current concentration: Burning, Electrochemical and Solid-State Letters 7 (2004) B21.
36) J.E. Houser, K.R. Hebert, The role of viscous flow of oxide in the growth of self-ordered porous anodic alumina films, Nature Materials 8 (2009) 415.
37) K.R. Hebert, S.P. Albu, I. Paramasivam, P. Schmuki, Morphological instability leading to formation of porous anodic oxide films, Nature Materials 11 (2012) 162.
38) S.J. Garcia-Vergara, P. Skeldon, G.E. Thompson, H. Habazaki, A flow model of porous anodic film growth on aluminium, Electrochimica Acta 52 (2006) 681.
39) G.D. Sulka, K.G. Parkoła, Anodising potential influence on well-ordered nanostructures formed by anodisation of aluminium in sulphuric acid, Thin Solid Films 515 (2006) 338.
40) G.D .Sulka, W.J. Stępniowski, Structural features of self-organized nanopore arrays formed by anodization of aluminum in oxalic acid at relatively high temperatures, Electrochimica Acta 54 (2009) 3683.
41) N. Kwon, N. Kim, J. Yeon, G. Yeom, I. Chung, Fabrication of ordered Au nanodot arrays utilizing anodic aluminum oxide templates formed on Si substrate, Journal of Vacuum Science & Technology B, 29 (2011) 031805.
42) J. Zhang, J.E. Kielbasa, D.L. Carroll, Controllable fabrication of porous alumina templates for nanostructures synthesis, Materials Chemistry and Physics, 122 (2010) 295.
43) T. Yanagishita, M. Masui, N. Ikegawa, H. Masuda, Fabrication of polymer antireflection structures by injection molding using ordered anodic porous alumina mold, Journal of Vacuum Science & Technology B, 32 (2014) 021809.
44) J.S. Hu, H.X. Ji, A.M. Cao, Z.X. Huang, Y. Zhang, L.J. Wan, A.D. Xia, D.P. Yu, X.M. Meng, S.T. Lee, Facile solution synthesis of hexagonal AlQ_3 nanorods and their field emission properties, Chemical Communications, 29 (2007) 3083.
45) T. Yanagishita, H. Masuda, High-throughput fabrication process for highly ordered through-hole porous alumina membranes using two-layer anodization, Electrochimica Acta, 184 (2015) 80.
46) K.D. Demadis, M. Paspalaki, J. Theodorou, Controlled release of bis (phosphonate) pharmaceuticals from cationic biodegradable polymeric matrices, Industrial & Engineering Chemistry Research 50 (2011) 5873.

47) K. Popov, H. Rönkkömäki, L.H. Lajunen, Critical evaluation of stability constants of phosphonic acids (IUPAC technical report), Pure and applied chemistry 73 (2001) 1641.
48) G.C. Wood, P. Skeldon, G.E. Thompson, K. Shimizu, A model for the incorporation of electrolyte species into anodic alumina, Journal of The Electrochemical Society 143 (1996) 74.
49) F. Le Coz, L. Arurault, L. Datas, Chemical analysis of a single basic cell of porous anodic aluminium oxide templates, Materials Characterization 61 (2010) 283.
50) L. González-Rovira, M. López-Haro, A.B. Hungría, K.E. Amrani, J.M. Sánchez-Amaya, J.J. Calvino, F.J. Botana, Direct sub-nanometer scale electron microscopy analysis of anion incorporation to self-ordered anodic alumina layers, Corrosion Science 52 (2010) 3763.

Figures

Fig. 1 Changes in the current density, j, with time, t, during anodizing of aluminum in a 0.2 M etidronic acid solution at 298 K and 255-265 V. The potential difference was increased linearly during the first 2.5 min of anodizing and was then held at each specific potential difference.

Fig. 2 Changes in the current density, j, with time, t, during anodizing of aluminum under the maximum potential differences without oxide burning in a 0.2 M etidronic acid solution at 288-323 K.

Fig. 3 SEM images of the surface of the aluminum specimen after a) first anodizing in a 0.2 M etidronic acid solution at 240 V and 303 K for 120 min and b) selective oxide dissolution in a CrO_3/H_3PO_4 solution at 353 K.

Fig. 4 SEM images of the nanostructured aluminum surface after 0.2 M etidronic acid anodizing at 205-310 V and 288-323 K for 120 min and 24 h and subsequent selective oxide dissolution.

Fig. 5 Changes in the current density, j, with time, t, during anodizing in a) a 1.0 M and b) 4.2 M etidronic acid solutions under the maximum potential difference condition.

Fig. 6 SEM images of the nanostructured aluminum surface fabricated via anodizing in a 1.0 M etidronic acid solution for 120 min at 170-245 V.

Fig. 7 SEM images of the nanostructured aluminum surface fabricated via anodizing in a 4.2 M etidronic acid solution at a) 165 V and b) 145 V.

Fig. 8 High- and low-magnification SEM images of OPA fabricated via etidronic acid anodizing at 165-260 V (a) in 4.2 M at 165 V and 313 K for 24 h, b) in 1.0 M at 205 V and 303 K for 24 h, c) in 1.0 M at 215 V and 298 K for 24 h, and d) in 0.2 M at 260 V and 298 K for 24 h). The insert figure shows the resulting FFT image obtained from the aluminum dimple array.

Fig. 9 a) An SEM image of the nanostructured aluminum surface fabricated via 0.2 M etidronic acid anodizing at 260 V for 24 h. b)-d) SEM images of b) OPA fabricated via two-step anodizing at 260 V and subsequent pore-widening at 298 K for c) 48 h, and d) 72 h in a 1.0 M etidronic acid solution. e)-g) SEM images of the fracture cross-section of the honeycomb nanostructure with narrow alumina walls (Fig. 8d).

Fig. 10 SEM image and diffraction pattern of physically thinned OPA fabricated two-step 1.0 M etidronic acid anodizing at 215 V and 298 K for 24 h and 120 min, and the corresponding STEM-EDS images of aluminum, oxygen, phosphorus, and carbon elements.

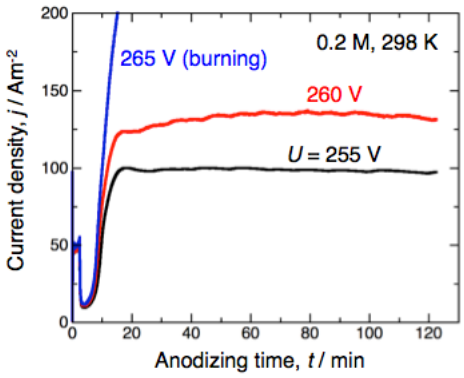
0.2 M, 298 K
265 V (burning)
260 V
U = 255 V
Current density, j / Am-2
Anodizing time, t / min
0
50
100
150
200
0
20
40
60
80
100
120

Figure 1.

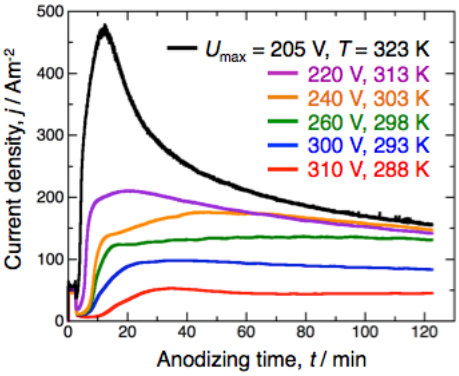
Current density, j / Am-2
Anodizing time, t / min
Umax = 205 V, T = 323 K
220 V, 313 K
240 V, 303 K
260 V, 298 K
300 V, 293 K
310 V, 288 K
0
100
200
300
400
500
0
20
40
60
80
100
120

Figure 2.

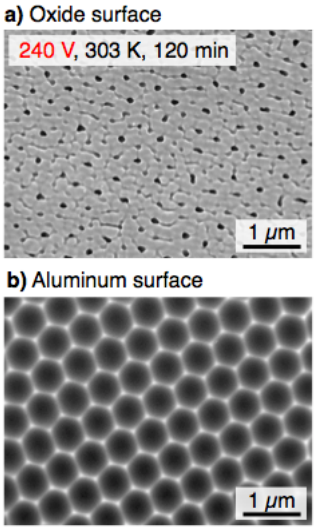

Figure 3.

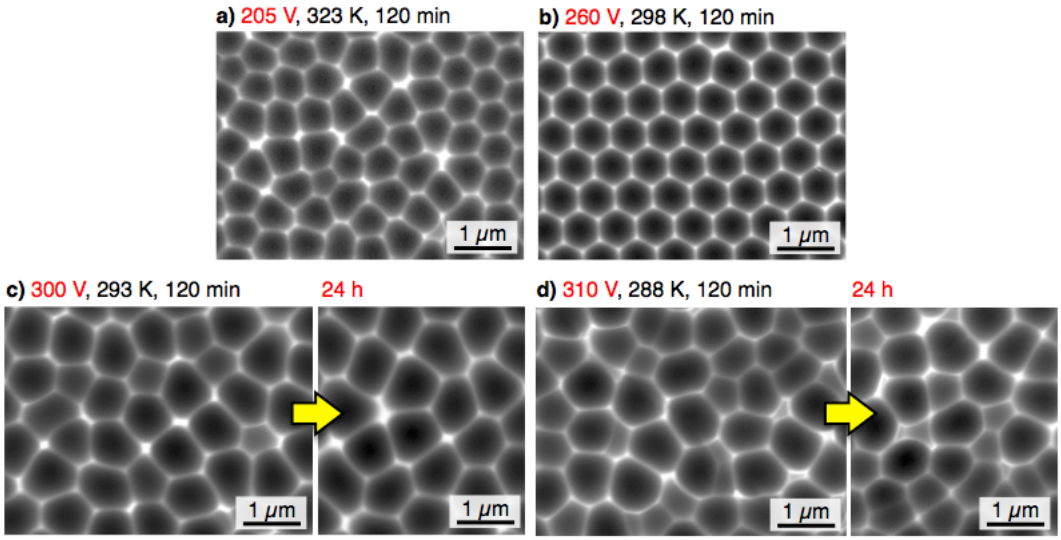
a) 205 V, 323 K, 120 min
b) 260 V, 298 K, 120 min
1 μm
1 μm
c) 300 V, 293 K, 120 min
24 h
d) 310 V, 288 K, 120 min
24 h
1 μm
1 μm
1 μm
1 μm

Figure 4.

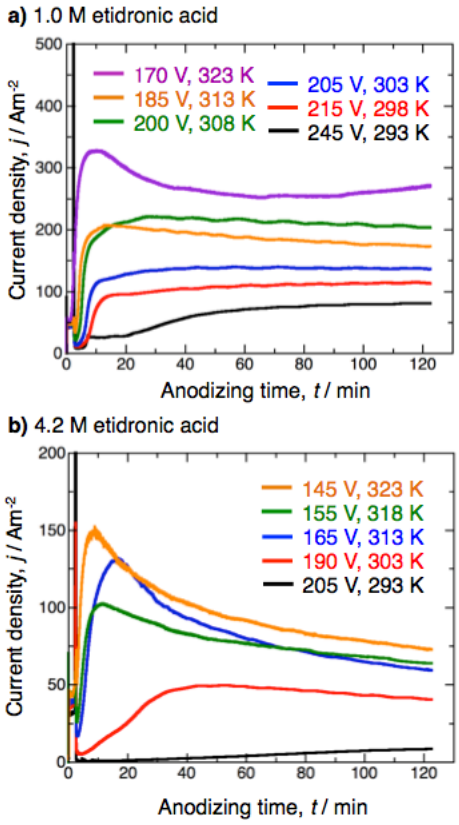
a) 1.0 M etidronic acid
170 V, 323 K
185 V, 313 K
200 V, 308 K
205 V, 303 K
215 V, 298 K
245 V, 293 K
Current density, j / Am-2
Anodizing time, t / min
b) 4.2 M etidronic acid
145 V, 323 K
155 V, 318 K
165 V, 313 K
190 V, 303 K
205 V, 293 K
Current density, j / Am-2
Anodizing time, t / min

Figure 5.

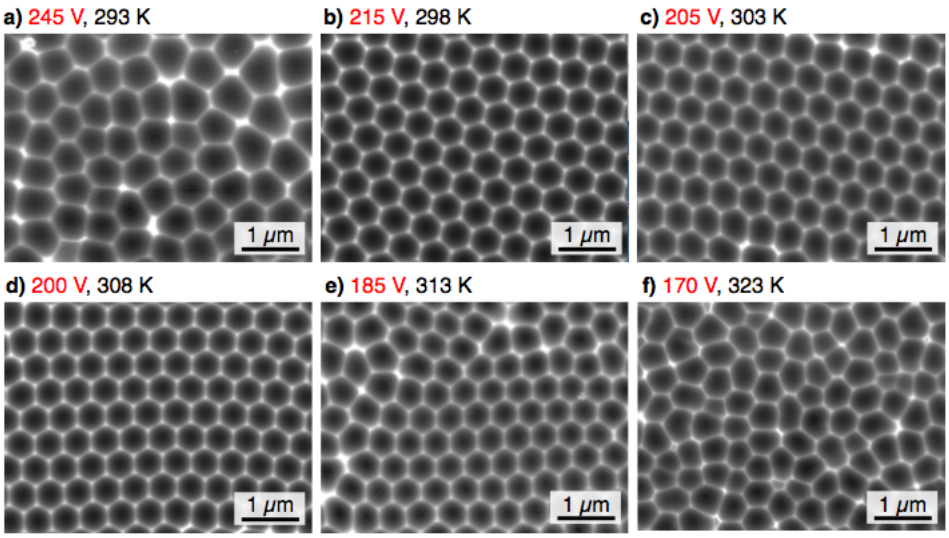
a) 245 V, 293 K
b) 215 V, 298 K
c) 205 V, 303 K
d) 200 V, 308 K
e) 185 V, 313 K
f) 170 V, 323 K
1 μm
1 μm
1 μm
1 μm
1 μm
1 μm

Figure 6.

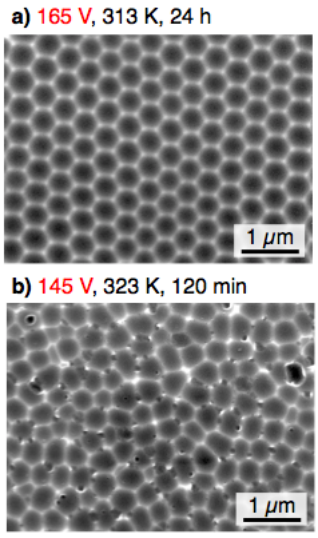

Figure 7.

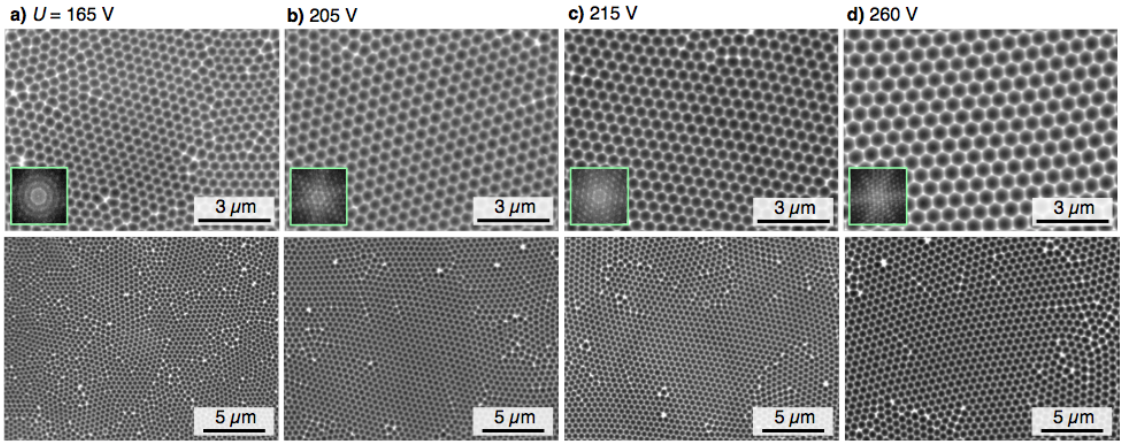

Figure 8.

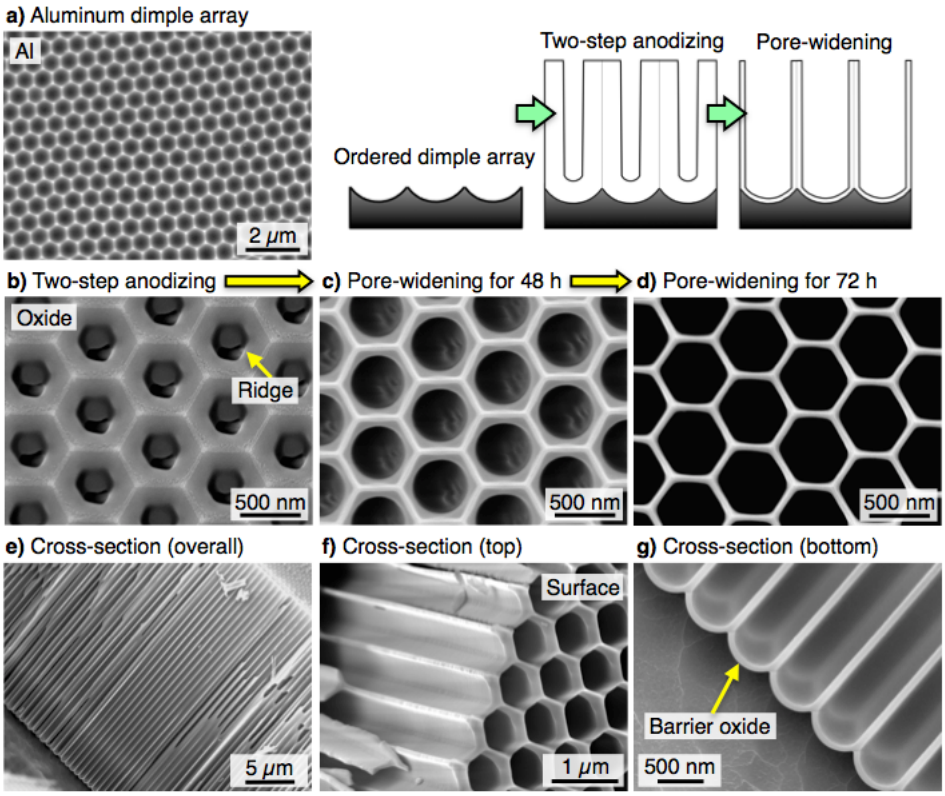
a) Aluminum dimple array
Al
2 μm
Two-step anodizing
Pore-widening
Ordered dimple array
b) Two-step anodizing
c) Pore-widening for 48 h
d) Pore-widening for 72 h
Oxide
Ridge
500 nm
500 nm
500 nm
e) Cross-section (overall)
f) Cross-section (top)
g) Cross-section (bottom)
Surface
Barrier oxide
5 μm
1 μm
500 nm

Figure 9.

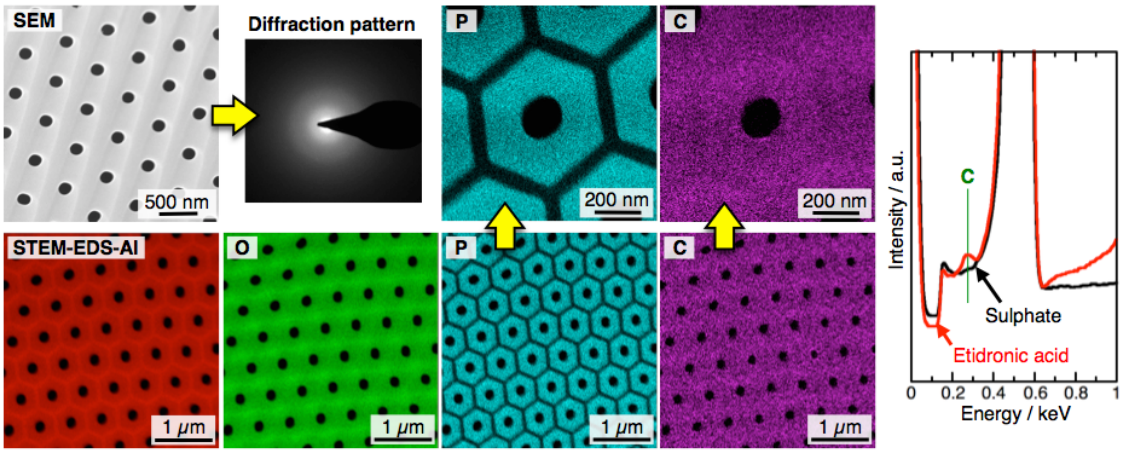
SEM
500 nm
Diffraction pattern
P
200 nm
C
200 nm
STEM-EDS-Al
1 μm
O
1 μm
P
1 μm
C
1 μm
Intensity / a.u.
C
Sulphate
Etidronic acid
0
0.2
0.4
0.6
0.8
1
Energy / keV

Figure 10.